Environmental Science: Atmospheres

ROYAL SOCIETY OF CHEMISTRY

PAPER

View Article Online
View Journal | View Issue



Cite this: *Environ. Sci.: Atmos.*, 2025, **5**, 1312

# Accretion product formation in the self- and cross-reactions of small β-hydroxy peroxy radicals

Sara E. Murphy, †*[a] John D. Crounse, [a] Andras Sun Poulsen,[b] Juliette E. Lipson,[a] Henrik G. Kjaergaard [b] and Paul O. Wennberg [ac]

The formation of a peroxide accretion product (ROOR) has recently been shown to be a significant channel in self- and cross-reactions of peroxy radicals ($RO_2$) in the gas-phase. Here, we examine the formation of this accretion product in the self- and cross-reactions of $RO_2$ derived from the OH-initiated oxidation of propene, *cis*-2-butene, and methylpropene in the presence of ethene. We measure the formation rate coefficient of the various accretion products in each system relative to the formation rate coefficient of the ethene-derived ROOR, which was measured in our previous work. We find that the accretion product forms in all of the studied self- and cross-reactions. The measured ROOR formation rate coefficient for the self-reaction decreases by approximately an order of magnitude with increasing substitution, with average rate coefficients of $4.7 \times 10^{-13}$ cm$^3$ molec$^{-1}$ s$^{-1}$ for primary hydroxy peroxy radicals, $2.7 \times 10^{-14}$ cm$^3$ molec$^{-1}$ s$^{-1}$ for secondary hydroxy peroxy radicals, and $8.0 \times 10^{-16}$ cm$^3$ molec$^{-1}$ s$^{-1}$ for the tertiary hydroxy peroxy radical. The cross-reaction rate coefficients of secondary and tertiary peroxy radicals with primary peroxy radicals are both higher than the corresponsing self-reactions, and also decrease with increasing radical substitution. We estimate the branching fraction to the formation of the ROOR for these peroxy radical self- and cross-reactions and find that branching fractions range from 0.03–0.33, with self- and cross-reactions of primary peroxy radicals having the highest branching fractions. Finally, we compare the reaction and ROOR formation rate coefficients of self- and cross-reactions of small $RO_2$, and determine that the arithmetic mean of self-reaction rate coefficients provides a suitable method for estimating cross-reaction rate coefficients.

Received 4th September 2025
Accepted 9th October 2025

DOI: 10.1039/d5ea00106d

rsc.li/esatmospheres



### Environmental significance

Organic peroxy radicals ($RO_2$), formed in the oxidation of volatile organic compounds (VOCs), play a crucial role in processes that affect the formation of atmospheric pollutants, including particulate matter and ozone. Reactions of these $RO_2$ can propagate or terminate the radical cycle, with each fate yielding distinct atmospheric impacts. The structural diversity of peroxy radicals in the atmosphere necessitates the study of the relationship between these reaction pathways and $RO_2$ structure, especially for accurate air quality and climate modeling. In this work, we quantify the formation rate coefficients for the formation of low volatility accretion products (ROOR) in the self- and cross-reactions of three small alkene-derived hydroxy peroxy radicals. We find that accretion products form in all the systems studied here and that the formation rate coefficients exhibit a decrease with increasing peroxy radical substitution. These results suggest that ROOR, which could play a role in the formation of particulate matter, can form for a variety of precursors, especially in the reactions of primary peroxy radicals.

## 1 Introduction

The oxidation of anthropogenic and biogenic hydrocarbons is one of the primary drivers of tropospheric chemical processes. After emission to the atmosphere, oxidation of these hydrocarbons is generally initiated by OH, $O_3$, or $NO_3$, followed by addition of $O_2$ to form peroxy radicals ($RO_2$).[1] The radical cycling and ultimate fate of these $RO_2$ has significant implications for, among other important processes, the formation of ozone and particulate matter.[2–4] In polluted areas such as urban centers, where nitrogen oxides ($NO_x$ = NO + $NO_2$) tend to be high, $RO_2$ primarily react with NO.[5,6] This reaction proceeds through either a radical recycling channel, in which $NO_2$ and an alkoxy radical (RO) are formed, or through the formation of an organic nitrate ($RONO_2$).[7,8] The former propagates the radical cycle that leads to ozone formation, while the latter can lead to the formation of secondary organic aerosol (SOA) and/or transport of $NO_x$ to regions removed from the original source.[9]

[a]*California Institute of Technology, Department of Geological and Planetary Sciences, Pasadena, CA, USA. E-mail: semurphy@ucla.edu*

[b]*University of Copenhagen, Department of Chemistry, Copenhagen, Denmark*

[c]*California Institute of Technology, Department of Engineering and Applied Sciences, Pasadena, CA, USA*

† Currently at the University of California, Los Angeles.

In regions where $NO_x$ is low, $RO_2$ will undergo unimolecular reaction[10] or bimolecular reactions with (primarily) $HO_2$ or other $RO_2$.[7,11] This chemistry is important in remote regions and is even becoming important in urban areas as $NO_x$ continues to decrease due to emission regulations.[12,13] The reaction of $RO_2$ with $HO_2$ can, similarly to the reaction with NO, lead to radical propagation (Reaction 1b and 1c) or radical termination (Reaction 1a) *via* the formation of a hydroperoxide (ROOH).[7]

$$RO_2 + HO_2 \rightarrow ROOH + O_2 \quad (1a)$$

$$\rightarrow RO + OH + O_2 \quad (1b)$$

$$\rightarrow R_{-H}{=}O + HO_2 + OH \quad (1c)$$

While Reaction 1a is the dominant pathway for most alkyl peroxy radicals, Reactions 1c and 1b have been observed to play an important role in the reactions of oxygenated peroxy radicals, including β-hydroxy peroxy radicals.[11] Although the reaction rate coefficient of $RO_2$ with $HO_2$ and the branching to products remains uncertain for many peroxy radicals, structure activity relationships suggest that the rate coefficient of the $RO_2 + HO_2$ reaction largely depends on the number of heavy atoms in the peroxy radical and exhibits little dependence on substitution or structure.[14]

The reaction of $RO_2$ with $R'O_2$ (the cross-reaction, Reaction 2) or with itself (the self-reaction, Reaction 2 with $R' = R$) proceeds primarily *via* three reaction pathways: the formation of two alkoxy radicals (Reaction 2a), the formation of an alcohol and a carbonyl (Reaction 2b and 2c), or the formation of a peroxide accretion product (Reaction 2d).[7,11]

$$RO_2 + R'O_2 \rightarrow RO + R'O + O_2 \quad (2a)$$

$$\rightarrow R'OH + R_{-H}{=}O + O_2 \quad (2b)$$

$$\rightarrow ROH + R'_{-H}{=}O + O_2 \quad (2c)$$

$$\rightarrow ROOR' + O_2 \quad (2d)$$

Generally, when $R' = R$, the rate of Reaction 2 decreases as the substitution of the peroxy radical increases, and increases with the addition of a hydroxy or acyl substituent.[11,15] Although this trend has been observed for self-reactions, the relationship between the kinetics of cross-reactions ($R \neq R'$) and self-reaction rate coefficients of the constituent peroxy radicals ($RO_2$ and $R'O_2$) remains poorly characterized.

The branching to the various products of Reaction 2 remains uncertain and has been the focus of substantial recent research. Most notably, it was previously widely accepted that Reaction 2d was negligible, as the resulting accretion products were not observed in laboratory oxidation studies and the proposed formation mechanism, involving an intersystem crossing, appeared unfavorable.[7,16,17] However, several recent studies have reported the formation of dimers (compounds with approximately twice the carbon number of the original peroxy radicals) in various oxidation systems. While some of these dimers are esters formed in the particle-phase[18] or *via* other gas-phase accretion mechanisms,[19] several of these products observed with chemical ionization mass spectrometry (CIMS) have masses consistent with the formation of the ROOR and are reported to form at appreciable rates that even approach the collision rate.[15,20–23] The formation of the ROOR is atmospherically significant both because it terminates the radical cycle (at least temporarily) and because these products have low volatilities and are likely to play a role in the formation of SOA. In fact, these compounds have been observed in the remote ambient environment in both the gas- and the particle-phase, demonstrating the role that these dimers play in particle formation.[24] Additionally, a possible fifth pathway for Reaction 2 leading to an alkoxy radical, carbonyl, and $HO_2$ was proposed for the self-reaction of the hydroxy ethyl peroxy radical,[25] further highlighting the need for additional study of the self-reaction for a variety of peroxy radical precursors.

Recently, accretion product formation has been reported for the self-reactions of ethyl peroxy,[26] hydroxy ethyl peroxy,[25] and propyl peroxy radicals,[27] with branching fractions of 10(±5)%, 23(±5)%, and 10(±5)%, respectively. In each of these studies, the identity of the dimers was confirmed to be the ROOR formed in Reaction 2d by either gas chromatography or vacuum ultraviolet (VUV) photoionization mass spectrometry. The observation of significant branching to accretion product formation in the self-reactions of these small peroxy radicals is compatible with recent studies of the self-reaction of ethyl peroxy radicals finding lower branching to alkoxy radical formation than previous studies.[28,29]

Despite these recent insights into the formation of accretion products *via* peroxy radical self- and cross-reactions, these studies have only been conducted for a limited number of peroxy radical precursors. There have been few studies that have systematically examined the relationship between the rate of accretion product formation and peroxy radical structure.[30] However, it is necessary to probe this relationship to predict the formation rate of the accretion product for the wide variety of peroxy radicals present in the atmosphere.

In this study, we begin to fill this gap by expanding on our previous study of the formation of the accretion product in ethene-derived hydroxy peroxy radical systems.[25] Specifically, we show that the accretion product forms in a variety of small-alkene-derived hydroxy peroxy radical self- and cross-reactions and measure the formation rate coefficient of the ROOR in each of these oxidation systems relative to the formation rate coefficient of the ethene-derived accretion product. By measuring this rate in the propene, methylpropene (isobutene), and *cis*-2-butene oxidation systems, we examine the relationship between accretion product formation and structure for these small hydroxy peroxy radicals. Using literature values for the absolute rate coefficients where available, we further estimate the branching to the accretion product for the reactions examined here.

# 2 Methods

## 2.1 Experimental design

In this study our goal is to quantify the formation of the peroxide accretion product for a series of small alkene-derived

peroxy radicals. In each case, the peroxy radicals of interest are formed by the addition of OH to the parent alkene, followed by the rapid addition of $O_2$ to form the peroxy radical:

$$R = R' + OH \xrightarrow{O_2} (OH)R - R'(O_2) \quad (3)$$

In all of our experiments, OH was generated by the photolysis of $H_2O_2$ (Reaction 4) *via* the illumination of eight Sankyo Denki G40T10 254 nm lamps for an average of 2 minutes. The photolysis rate of $H_2O_2$ under these conditions in our 800 liter FEP Teflon environmental chamber is $3.0(\pm0.5) \times 10^{-4}$ $s^{-1}$.[25]

$$H_2O_2 \xrightarrow{h\nu} OH + OH \quad (4)$$

In several of the experiments reported here, the fraction of alkene reacted over the photolysis period was estimated by simultaneously observing the formation of glycolaldehyde in the reaction of ethylene glycol with OH (Reaction 5).

$$HOCH_2CH_2OH + OH \xrightarrow{O_2} HOCH_2CH(O) + HO_2 + H_2O \quad (5)$$

The recommended value for the reaction of ethylene glycol with OH is $1.45 \times 10^{-11}$ $cm^3$ $molecule^{-1}$ $s^{-1}$ ($\Delta \log k = \pm 0.20$).[31] In experiments where ethylene glycol was used as a probe of OH exposure ([OH] $\times$ $\Delta t$), 20–70 ppbv of ethylene glycol was injected. The OH exposure was then calculated using the measured production rate of glycolaldehyde from a known concentration of ethylene glycol. This calculation yielded estimated OH exposures ranging between 0.4–6.0 $\times$ $10^9$ molecules $cm^{-3}$ s across the various precursors and conditions used here. In these systems, the OH exposure was also calculated using our photochemical box model, and values agree within a factor of 2. Therefore, in experiments in which no OH probe was used, the photochemical box model was used to estimate the fraction of reacted alkene.

We performed a suite of experiments at ambient pressure ($P$ = 753 $\pm$ 3 torr) and room temperature ($T$ = 295.2 $\pm$ 0.6 K) to quantify the product of the self-/cross-reaction rate coefficient ($k_2$) times the branching fraction leading to accretion products ($\alpha_{2d}$) of several $RO_2$ + $R'O_2$ reactions relative to the value measured for ethene in our previous work ($k_2\alpha_{2d} = 5.5(\pm2.6) \times 10^{-13}$ $cm^3$ $molecule^{-1}$ $s^{-1}$).[25] We oxidized mixtures of ethene with propene, 2-methylpropene (isobutene), or *cis*-2-butene and observed the formation of accretion products from all combinations of the resulting $RO_2$ + $R'O_2$ reactions. To estimate $k_2\alpha_{2d}$, experiments were performed under conditions where most (>90%) of the peroxy radicals reacted with $HO_2$ *via* Reaction 1a to form ROOH. Under these conditions, the ratios of the observed concentrations of ROOH provide a constraint on the ratios of the parent $RO_2$ concentrations (eqn (6)):

$$\frac{[RO_2]_{HC}}{[RO_2]_E} = \frac{[ROOH]_{HC} k_{1,E} \alpha_{1a,E}}{[ROOH]_E k_{1,HC} \alpha_{1a,HC}} \quad (6)$$

where HC = non-ethene hydrocarbon, E = ethene, $k_{1,E}$ and $k_{1,HC}$, are the rate coefficients of Reaction 1 for ethene and non-ethene hydrocarbons, respectively, and $\alpha_{1a,E}$ and $\alpha_{1a,HC}$ are the branching fractions to ROOH. According to our photochemical box model, eqn (6) is accurate to within 7% under the conditions of our experiments.

To ensure that the $[HO_2]/[RO_2]$ ratio satisfies the condition that >90% of $RO_2$ react with $HO_2$, we add sufficient concentrations of methanol such that the reaction of OH with methanol exceeds the reaction of OH with the alkenes, as has been described previously.[25] In the oxidation experiments performed in this study, the relative concentrations of methanol and parent hydrocarbon yielded steady state $[HO_2]/[RO_2]$ ratios above 2.0 (as estimated by our box model). Because the rate coefficients for the reaction of $RO_2$ with $HO_2$ ($k_1$) are generally more than an order of magnitude faster than the rate coefficients of the self- and cross-reactions ($k_2$) for the systems studied here, the requirement that the peroxy radicals react overwhelmingly with $HO_2$ is satisfied under these conditions.

A measurement of $k_2\alpha_{2d}$ for each alkene can then be obtained from the measured ratio of the accretion product of interest to the ethene-derived accretion product. For the self-reaction of a given isomer of a peroxy radical derived from a non-ethene hydrocarbon (in this case propene, methylpropene, or *cis*-2-butene), the $k_{2,HC}\alpha_{2d,HC}$ value is given by eqn (7), where the ratio of the $RO_2$ concentrations is obtained from eqn (6):

$$k_{2,HC}\alpha_{2d,HC} = k_{2,E}\alpha_{2d,E}\left(\frac{[RO_2]_E}{[RO_2]_{HC}}\right)^2\left(\frac{[ROOR]_{HC}}{[ROOR]_E}\right) \quad (7)$$

If the accretion product of interest is formed *via* the cross-reaction of two different isomers of the same non-ethene hydrocarbon ($HC_a$ and $HC_b$), this equation becomes:

$$k_{2,HC_{a,b}}\alpha_{2d,HC_{a,b}} = k_{2,E}\alpha_{2d,E}\left(\frac{[RO_2]_E}{[RO_2]_{HC_a}}\right)\left(\frac{[RO_2]_E}{[RO_2]_{HC_b}}\right)\left(\frac{[ROOR]_{HC_{a,b}}}{[ROOR]_E}\right) \quad (8)$$

Finally, for determination of the $k_2\alpha_{2d}$ value for the cross-reaction between an isomer of a non-ethene hydrocarbon and ethene, eqn (7) reduces to:

$$k_{2,HC+E}\alpha_{2d,HC+E} = k_{2,E}\alpha_{2d,E}\left(\frac{[RO_2]_E}{[RO_2]_{HC}}\right)\left(\frac{[ROOR]_{HC+E}}{[ROOR]_E}\right) \quad (9)$$

Using eqn (7)–(9), we calculate the $k_2\alpha_{2d}$ values for all of the self- and cross-reactions of the peroxy radical systems studied here.

Our estimate of $k_2\alpha_{2d}$ is particularly sensitive to $k_1$ and $\alpha_{1a}$. $k_1$ is estimated here using the structure activity relationship (SAR) found in Wennberg *et al.*[14] This rate coefficient has been measured for the primary peroxy radical derived *via* the oxidation of 2-methylpropene ($k_1 = 1.5(\pm0.9) \times 10^{-11}$ $cm^3$ $molecule^{-1}$ $s^{-1}$)[6] and the secondary peroxy radical derived *via* the oxidation of *cis*-2-butene ($k_1 = 1.5(\pm0.4) \times 10^{-11}$ $cm^3$ $molecule^{-1}$ $s^{-1}$).[5] These measured values are the same as those values predicted by the structure–activity relationship within error ($1.6 \times 10^{-11}$ $cm^3$ $molecule^{-1}$ $s^{-1}$ at 295 K for both

compounds), and so the SAR values are used in all cases for consistency.

Estimates of $\alpha_{1a}$ were derived from the concentration of ROOH formed in the high $HO_2$ experiments. In these experiments, the amount of ROOH formed divided by the concentration of the reacted alkene is approximately equal to the branching fraction of Reaction 1a (eqn (10)).

$$\frac{\Delta[\mathrm{ROOH}]}{-\Delta[\mathrm{HC}]} = \alpha_{1a,\mathrm{HC}} \quad (10)$$

According our photochemical box model, for the conditions of our experiments, eqn (10) is accurate to better than 9%. There is additional error induced by the estimation of the reacted alkene used in the calculation of $\alpha_{1a}$. We assign the modelled OH exposures, and by extension the fraction of reacted alkene, an uncertainty of 50%. This is by far the largest source of uncertainty in the estimation of $\alpha_{1a}$. Further, this error is much larger than the uncertainties in the values of $k_1$. Therefore, we assign the $\alpha_{1a}$ an uncertainty of 50% and the overall calculation of $k_2\alpha_{2d}$ a corresponding uncertainty of 50%.

Finally, to assign elution temperatures to ROOR isomers in the gas chromatograms, we performed experiments where we did not add methanol. This maximized the fraction of $RO_2$ undergoing self- and cross-reactions and thus the signal-to-noise ratios of the resulting chromatograms. These experiments are labeled 'high $RO_2$' in the discussion below and generally contained $[HO_2]/[RO_2]$ ratios that were much less than 1.

### 2.2 Instrumentation

All measurements in this study were conducted using the Caltech gas chromatograph chemical ionization mass spectrometer (GC-CIMS). This instrument has been described in detail previously,[32] but a brief description is given here.

The Caltech GC-CIMS uses a high resolution ($m/\Delta m \sim 3000$) time-of-flight mass spectrometer with $CF_3O^-$ reagent to ionize and detect analytes. $CF_3O^-$ is produced by flowing $CF_3OOCF_3$ in $N_2$ through a polonium-210 ionizer (NRD, LLC). In direct sampling mode, the analyte gas is sampled at approximately 2000 sccm, and 180 sccm of this sample passes through a Teflon-coated metal critical orifice into a Teflon-coated glass flow tube that is maintained at a pressure of approximately 35 mbar. Here, the sample is diluted with $N_2$ and turbulently mixes with 380 sccm flow of $N_2$ from the ion source. The analytes are then ionized by reaction with the reagent ion. For most of the compounds considered here, the analyte forms a cluster with the reagent ion that appears at a mass-to-charge ratio ($m/z$) of the molecular weight (mw) of the compound plus the mass of $CF_3O^-$ ($m/z$ = mw + 85). However, analytes may also undergo a fluorine transfer reaction, thus appearing at a mass-to-charge ratio equal to the molecular weight of the analyte plus the mass of fluorine ($m/z$ = mw + 19). Although fragmentation in this ionization scheme is minimal compared to the fragmentation observed in other chemical ionization schemes, some compounds still lead to characteristic fragments. For example, organic hydroperoxides characteristically form fragment ions at $m/z$ 63 ($FCO_2^-$) and $m/z$ 81.[33–35] The ionized analytes are then directed into the mass spectrometer through a pinhole and a conical hexapole ion guide, where they are subsequently detected. Signals were collected for mass-to-charge ratios between $m/z$ 19 and $m/z$ 396.

The metal-free, low-pressure gas chromatograph consists of a 2 meter fused silica column (Restek RTX-1701) that is cooled *via* the expansion of liquid $CO_2$ and heated with resistance heaters. During GC sampling, the analyte gas was sampled at approximately 1200 sccm and diluted by a factor of 2–6 *via* the addition of dry nitrogen flow. A fraction of the diluted sample flow was passed through a small trap upstream of the column, where analytes were collected. Trapping temperatures (−10 °C, −20 °C, or −30 °C), trapping times (2–10 min), and dilution factors were chosen to maximize the concentration of analyte trapped while avoiding the trapping of water. After trapping, the temperature was increased to 130 °C at a pre-determined temperature program with 5 sccm of nitrogen flowing through the trap and column. The effluent was then directed into the flow tube with a 200 sccm pickup flow of nitrogen and detected by the CIMS. The CIMS automatically switches between sampling from the GC and sampling directly from the chamber. A complete list of the temperature ramps and trapping conditions used in these experiments is given in the SI. For each experiment, a background chromatogram was taken prior to the initiation of oxidation and three chromatograms were taken after the oxidation period.

### 2.3 CIMS calibration and GC collection and transmission efficiencies

The sensitivity of the CIMS to most compounds in this study was estimated *via* calculation of their ion-molecule collision rates relative to that of ethylene glycol, for which we have extensive calibration data. This procedure is described in detail in previous work,[25] but is briefly summarized here. The CIMS instrument used in this work implements a transverse ionization scheme that results in a short interaction time (approximately 5 ms) between the analyte and reagent ions. In this configuration, the sensitivity of the analyte is approximately proportional to the ion-molecule collision rate, after accounting for the fraction of these collisions that result in ionization of the analyte, the transmission efficiency of the resulting ions, and any fragmentation of the analyte in the ionization process. Further, this sensitivity also depends on the total number of reagent ions (which includes $CF_3O^-$ and its clusters with $H_2O$ and $H_2O_2$). Since the fraction of reagent ions reacting with analytes is small, we can normalize the analyte signals to the total reagent ion signal. Specifically, to remain in a linear counting regime, we normalize our signals to the sum of the signals of the isotopic analogues of the reagent ions ($m/z$ = 86, 104, and 120). The resulting signals are then proportional to the concentration of the analyte in the sample. In prior work, we measured a sensitivity of $2.5(\pm0.2) \times 10^{-4}$ normalized counts/pptv of the CIMS to ethylene glycol.[25]

$CF_3O^-$ binds strongly to multifunctional organic compounds,[36] such that the fraction of the analyte that undergoes ionization generally depends on the ion-molecule collision rate. For analytes that form weakly bound clusters (such as $H_2O_2$), not every collision results in the formation of a stable ion cluster. Such analytes are identified by probing the relationship between sensitivity and temperature and humidity, as the sensitivity of these compounds tends to exhibit a negative dependence on temperature and often a complex dependence on water concentration.[37] The efficiency of cluster formation following collision may decrease due to fragmentation of the product ion and/or subsequent ligand exchange reactions. In our previous work on the ethene-derived peroxy radical self-reaction, we found that the clusters of the resulting $RO_2$ products with the reagent ion were well bound and exhibited little fragmentation. Due to the similar sizes and chemical structures of the compounds studied here and those probed in the prior study, we assume that the compounds considered in this study are similarly well-bound, and thus that sensitivities scale with ion-molecule collision rates. The sensitivities of the compounds measured in this study are estimated by calculating their ion-molecule collision rates relative to ethylene glycol and using this scaling factor to obtain the sensitivity from the measured ethylene glycol sensitivity. The calculated ion-molecule collision rates relative to ethylene glycol are given in the SI and are obtained using the methods outlined in Su *et al.*[38] and quantum calculations of the conformer-weighted dipole moments and polarizabilities of the relevant compounds.[39] The calculated rates vary by ±9% for the molecules of interest here.

The GC elution efficiency, which encompasses the combined effects of collection and transmission efficiencies, was determined for each compound by comparison of the sum of the total GC signal to the average CIMS signal obtained in direct sampling without chromatographic separation. These values were determined for a variety of trapping temperatures, and thus a variety of collection efficiencies. The measured elution efficiencies ranged between 10% and 100% – the lowest values generally reflect small ketones and alcohols for which the trapping was inefficient. The average elution efficiencies of each of the relevant compounds are given in the SI.

### 2.4 Isomer distribution and peak fitting

The calculations of the self- and cross-reaction rate coefficients for the individual isomers of the peroxy radicals studied here required separation of the resulting $RO_2$ products in the gas chromatograph and the subsequent quantification of their concentrations. The relative concentrations of each of these isomers was determined by fitting each peak using a modified open-source MATLAB peak-fitting function.[40] The GC peaks from our instrument were fit with exponentially-broadened Gaussian peak shapes with variable peak widths and exponential time constants. The peak widths and time constants that minimized the total error for these fits were determined by performing a bootstrap best-fit procedure in which 1000–10000 trials were performed with the parameters randomly varied to within ±50% of the initial guess. The resulting best-fit parameters, which are provided in the SI for the experiments discussed here, were then used to calculate the area under each chromatographic peak.

To account for elution efficiencies less than unity in the GC, we did not calculate the concentration of each isomer directly from the integrated GC signal. Rather, the relative proportions of the isomers of each compound were calculated using the ratio between the fitted peak areas. These proportions were subsequently multiplied by the total CIMS direct-sampling signal to determine the concentrations of each isomer. In this calculation, we implicitly assume that the direct-sampling signal represents the total concentration of a given set of isobaric isomers and that the trapping and transmission efficiencies of these different isomers are the same.

### 2.5 Reagent preparation

$H_2O_2$ (30% by mass, Macron Fine Chemicals) was measured by weight into a pre-weighed three-way glass vial and injected into the chamber by evaporating this weighed sample with dry air flowing at 20 SLM. The glass vial was reweighed following injection to ensure complete evaporation of the sample. Ethylene glycol (Sigma-Aldrich) was injected in a similar manner, with the glass vial partially immersed in warm water to ensure evaporation of the sample.

Ethene (≥99.5%, Sigma-Aldrich), methanol (≥99.9%, Sigma-Aldrich), 2-methylpropene (99%, Sigma Aldrich), *cis*-2-butene (≥99%, Sigma Aldrich), and propene (≥99%, Sigma Aldrich) samples were measured into 500 mL glass bulbs *via* a manometric apparatus in which the bulb was attached simultaneously to a vacuum/$N_2$ system and to the reagent source. The desired concentration of the relevant hydrocarbon was then obtained by serial dilution with pressure measurements conducted using pressure sensors (MKS 1000 and 10 Torr baratron pressure transducers). The purity of the samples and the concentrations measured using manometry were confirmed by taking IR spectra in a 19 cm pyrex FTIR cell with $CaF_2$ windows and fitting the resulting spectra to cross sections obtained from the PNNL IR Database.[41] The measurements taken with manometry and the concentration calculated from the FTIR spectra agree to within 30%.

## 3 Results and discussion

### 3.1 2-Methylpropene

The expected products of the $NO_x$-free OH-initiated oxidation of 2-methylpropene are shown in Scheme 1. Two peroxy radical isomers, a tertiary peroxy radical (tMP) and a primary peroxy radical (pMP), are formed *via* the major and minor OH addition reactions, respectively. Hydrogen abstraction by OH has been found to account for <5% of the overall reaction of 2-methylpropene and is therefore neglected in this analysis.[1,42] Representative chromatograms of the major accretion and hydroperoxide products are given in Fig. 1.

Two isomers of the ROOH product are expected to form: that derived from the primary $RO_2$, pMP-ROOH, and that derived from the tertiary $RO_2$, tMP-ROOH. In experiments with high

 

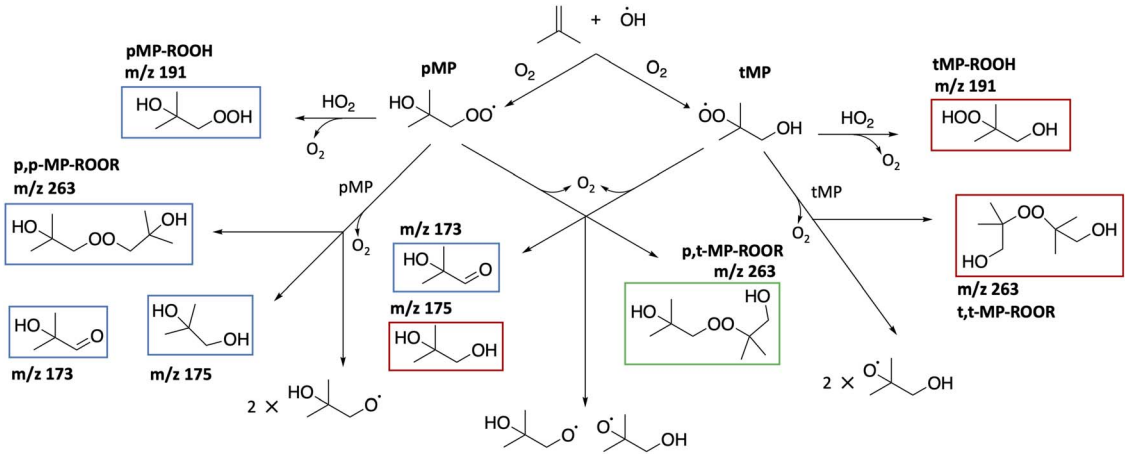


Scheme 1 Reaction scheme for the oxidation of 2-methylpropene by OH in the presence of $O_2$. Stable products that can be observed with the $CF_3O^-$ GC-CIMS are boxed and color-coded such that products that are derived from the primary peroxy radical are in blue, those derived from the tertiary peroxy radical are in red, and the product formed from the cross-reaction of the primary and tertiary peroxy radical is in green. Each product is labelled with the *m/z* of the $CF_3O^-$ cluster ion observed in our CIMS, which is equal to the molecular weight + 85. In the presence of $O_2$, the alkoxy radicals shown will decompose to formaldehyde, acetone, and $HO_2$.

$HO_2/RO_2$ ratios $\left(\frac{HO_2}{RO_2} > 2\right)$, the distribution of these products is expected to reflect the ratio of the production rates of the pMP and tMP due to the lack of other competitive loss channels, *i.e.* all $RO_2$ react with $HO_2$ to form ROOH.[14] We expect the observed ratios of the ROOH products to match those measured in Teng *et al.*, which were measured under conditions where $RO_2$ self-reaction chemistry was negligible and are taken here as an accurate measurement of the relative production rates of the peroxy radical isomers (21(±2)%/79(±2%) for pMP-ROOH/tMP-ROOH).[42] In the high $HO_2$ experiments presented in this study, the average distribution of pMP-ROOH/tMP-ROOH is 16(±1)%/84(±1)% (Fig. 1c). This is within 5% of the distribution found by Teng *et al.*, confirming that the primary loss of $RO_2$ in these

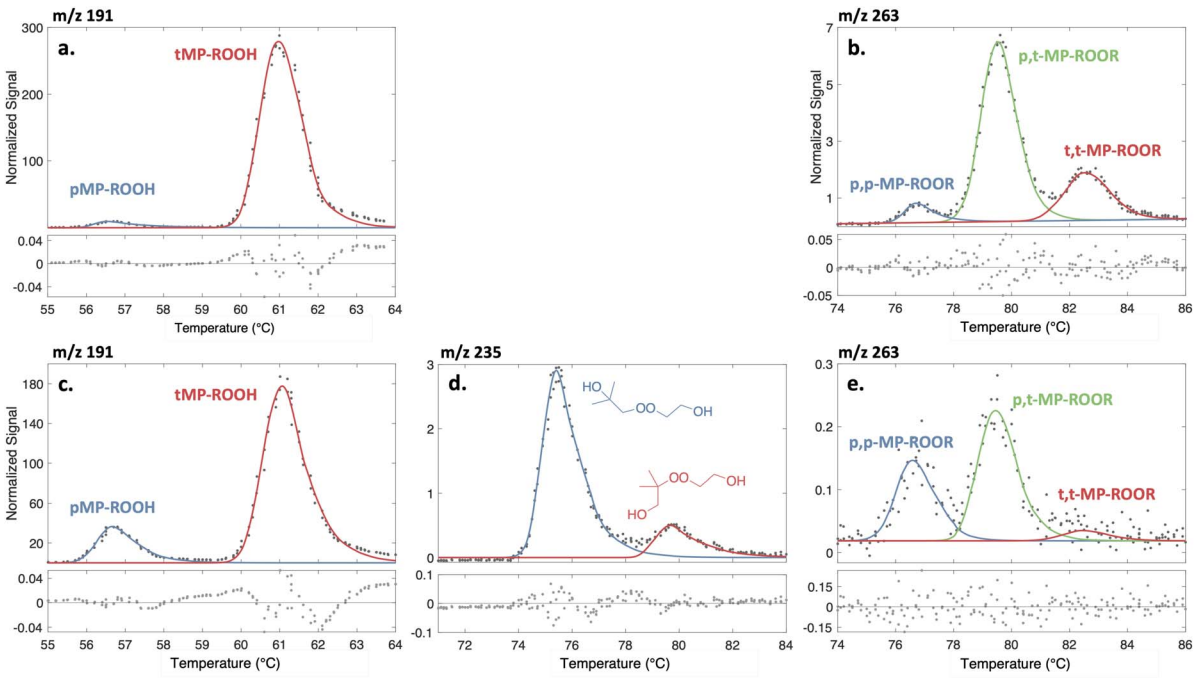


Fig. 1 Representative chromatograms of ROOH (a and c) and ROOR (b, d, and e.) products formed in the oxidation of 2-methylpropene in experiments with high $RO_2/HO_2$ ratios (top row) and high $HO_2/RO_2$ ratios (bottom row). Experiments represented in the bottom row also included ethene. The experimentally measured signal is given as dark gray dots, while the colored lines are the bootstrap best fits of the chromatographic data. The corresponding structures are the assignments of these peaks. Below each chromatogram are plots of the residuals of the best fits given as fractions of the maximum peak value.

experiments is reaction with $HO_2$ (although some loss due to $RO_2$ self-reaction chemistry is still expected).

In the high $RO_2$ regime $\left(\frac{HO_2}{RO_2} < 1\right)$, the fraction of ROOH as pMP-ROOH is significantly lower than that observed in the high $HO_2$ condition, with an average distribution of 3(±1)% pMP-ROOH and 97(±1)% tMP-ROOH (Fig. 1a). Under these conditions, the distribution of pMP-ROOH and tMP-ROOH is significantly altered by the loss rates of tMP and pMP $RO_2$ due to self- and cross-reaction chemistry. The dramatic decrease in the production of pMP-ROOH relative to tMP-ROOH when $RO_2$ self- and cross-reactions are prominent is consistent with previous observations that the rate of self- and cross-reactions of primary peroxy radicals are rapid compared to the self-reactions of tertiary peroxy radicals.[11]

Under the high $RO_2$ condition, three isomers at the mass of the accretion product (*m*/*z* 263) are observed, consistent with the expected products outlined in Scheme 1. Therefore, we see that the accretion product is formed at appreciable rates in all three of the possible self- and cross-reactions in this oxidation system. The isomeric distribution of the methylpropene-derived accretion product formed in Reaction 2 is influenced by the competing factors of peroxy radical abundance and reaction rate. Although the branching to the formation of tertiary peroxy radicals in the OH-initiated oxidation of 2-methylpropene is approximately 80%,[42] and therefore tMP will be more abundant than pMP, the self-reactions of tertiary peroxy radicals are generally several orders of magnitude slower than those of primary peroxy radicals.[7,11]

These competing factors are evident in the distribution of the ROOR isomers under varying conditions, as shown in Fig. 1. The peak assignments given in Fig. 1 follow the observation that, in the Caltech GC-CIMS instrument, compounds with primary –OH groups elute at higher temperatures than those with tertiary –OH groups due to the corresponding decrease in interaction strength between the analyte and the column.[43] The ROOR produced in the cross-reaction of pMP and tMP (p,t-MP-ROOR) is produced in the highest proportion under high $RO_2$ conditions, constituting on average 69(±4)% of the total concentration of methylpropene-derived accretion products (Fig. 1b). t,t-MP-ROOR constitutes 23(±3)% of this signal, with 7(±2)% of the signal on average attributed to the peroxide formed in the self-reaction of pMP (p,p-MP-ROOR) (Fig. 1b). Clearly, the cross-reaction between pMP and tMP is favored as a sink of tMP over the self-reaction. However, pMP reacts quickly, such that the steady state concentration of pMP is quite low, as demonstrated by the low proportion of pMP-ROOH relative to tMP-ROOH. Therefore, a significant concentration of t,t-MP-ROOR is formed despite the slow self-reaction of tertiary peroxy radicals. These observations are further quantified and discussed in the section on ROOR formation rate coefficients below.

In experiments with high $HO_2/RO_2$ ratios, 2-methylpropene and ethene were oxidized together to measure the relative production rates of the ethene- and methylpropene-derived accretion products, as described in the Methods section.

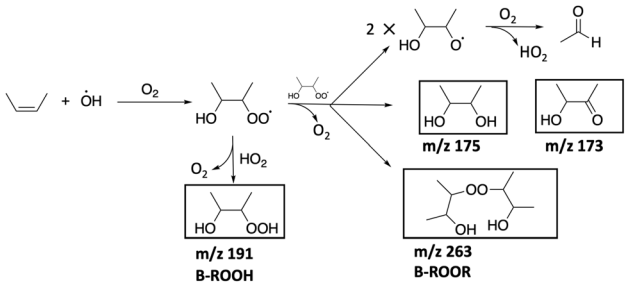


Scheme 2 Reaction scheme for the oxidation of *cis*-2-butene by OH in the presence of $O_2$. Stable products that can be observed with the $CF_3O^-$ GC-CIMS are boxed and labelled with the *m*/*z* at which they are observed. For simplicity, stereosiomers are not distinguished.

Under these conditions, the proportion of t,t-MP-ROOR decreases appreciably to between 0–5% of the total methylpropene-derived ROOR concentration (Fig. 1e). The signal-to-noise ratio of this peak is very low, with the peak indistinguishable from the noise in some cases – therefore, significant uncertainty is assigned to this fitted peak area. On the other hand, the concentrations of p,p-MP-ROOR and p,t-MP-ROOR are comparable, with average proportions of 37(±1)% and 61(±2)%, respectively. Further, two compounds are observed at *m*/*z* 235, consistent with accretion products formed in the cross-reactions of 2-methylpropene and ethene-derived peroxy radicals (E,pMP-ROOR and E,tMP-ROOR, Fig. 1d). These compounds are produced in unequal proportions, with a distribution of 78(±3)%/22(±3)%. We assign the less prominent peak to E,tMP-ROOR by comparison to the elution temperature of the accretion product formed in the oxidation of t-butanol in the presence of ethene (see Fig. S3). This assignment also aligns with previous observations that isomers with primary OH groups elute at warmer temperatures than isomers with more substituted OH groups. The prominence of E,pMP-ROOR suggests that the formation of the accretion product in the cross reaction of the ethene-derived peroxy radical (pE) and pMP is quite fast. These observations are discussed further in the section on ROOR formation rate coefficients.

### 3.2 *Cis*-2-butene

The simplified mechanism of the $NO_x$-free OH-initiated oxidation of *cis*-2-butene is given in Scheme 2. Stable products that are observed *via* clustering with $CF_3O^-$ in the Caltech GC-CIMS are boxed and labeled with the corresponding *m*/*z*. The H-abstraction pathway is expected to be negligible (<5% of the total reaction with OH). In contrast to the 2-methylpropene system, the symmetry of the parent molecule yields only one structural isomer of the peroxy radical. However, four stereoisomers of the peroxy radical (two diasteromers, with accompanying enantiomers) are possible, and these will react to form distinct ROOH, ROOR, and diol products that have the potential to be chromatographically separated (for simplicity, stereoisomers are not distinguished in Scheme 2). Representative chromatograms of the resulting peroxide, hydroperoxide, and diol products are given in Fig. 2.

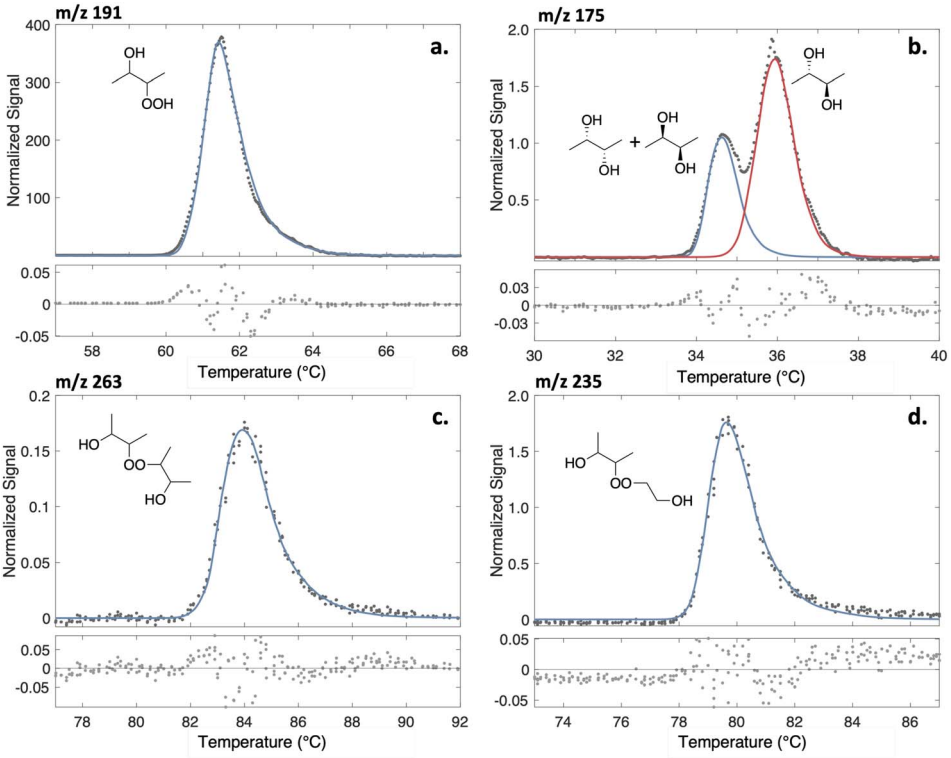


Fig. 2 Gas chromatograms of several important compounds produced in the oxidation of *cis*-2-butene by OH in the presence of $O_2$ and ethene, including (a) ROOH, (b) diol, (c) ROOR formed in the self-reaction, and (d) ROOR formed in the cross-reaction with ethene. (a) and (d) are chromaograms from a high $RO_2$ experiment, and (b) and (c) are chromatograms from a high $HO_2$ experiment. Experimentally measured signals are given in gray dots, while the bootstrapped best fits to these peaks are given in colored lines. The provided structures correspond to the assigments of these peaks. Below each chromatogram the residuals of the best fits are plotted as a fraction of the maximum peak signal. The chromatograms in (a) and (b) are corrected for significant tailing – this correction is described in the SI.

Two diasteromers of the peroxy radical are formed, the reactions of which are expected to produce multiple stereoisomers of the resulting products (B-ROOH, B-ROOR, and 2,3-butanediol). In agreement with this expectation, two closely separated peaks are observed in the chromatogram at *m*/*z* 175, the mass-to-charge ratio at which 2,3-butanediol appears in the CIMS, with a distribution of 34(±8)%/66(±8)% in the high $RO_2$ $\left(\frac{[HO_2]}{[RO_2]} < 1\right)$ experiments (Fig. 2b). Comparison of this chromatogram with those of *meso* and R,R-2,3-butanediol standards confirms the identity of these peaks as the stereoisomers of 2,3-butanediol (see Fig. S1). The elution temperature of the minor peak is consistent with a mixture of the enantiomers (R,R and S,S), while the major peak is consistent with the *meso* compound (Fig. 2). The observation that the entatiomers contribute a smaller fraction to the overall butanediol concentration than the *meso* compound is consistent with theoretical calculations suggesting that, due to stronger hydrogen bonding in the intermediate alkoxy enantiomer complex, the *meso* compound has a faster hydrogen shift rate than the enantiomer pair.[44] In contrast, multiple peaks are not observed at the masses associated with B-ROOH and B-ROOR. Some of these chromatograms exhibit a larger peak width than other compounds that elute at similar temperatures (Table S8), suggesting that this is likely due to a lack of chromatographic separation.

As in the analysis of the 2-methylpropene system, high $HO_2$ experiments $\left(\frac{[HO_2]}{[RO_2]} > 2\right)$ were performed with a mixture of ethene and *cis*-2-butene to directly compare the formation rates of the accretion products. The distribution of the stereosiomers of butanediol does not change (within error) under this condition, with an average distribution of the enantiomers to the *meso* compound of 31(±6)%/69(±6)%. Without chromatographic separation of the stereoisomers of B-ROOH, it is difficult to draw any definitive conclusions from this observation of the butanediol isomeric distribution. In these experiments, accretion products formed in the cross reactions between the ethene- and *cis*-2-butene-derived peroxy radicals (*m*/*z* 235) were observed alongside accretion products resulting from the corresponding self-reactions (*m*/*z* 263), as shown in Fig. 2c and d, respectively. The measured formation rate coefficients of these compounds is discussed in the section on ROOR formation rates.

### 3.3 Propene

The mechanism of the OH-initiated $NO_x$-free propene oxidation system is given in Scheme 3. Two structural isomers of the

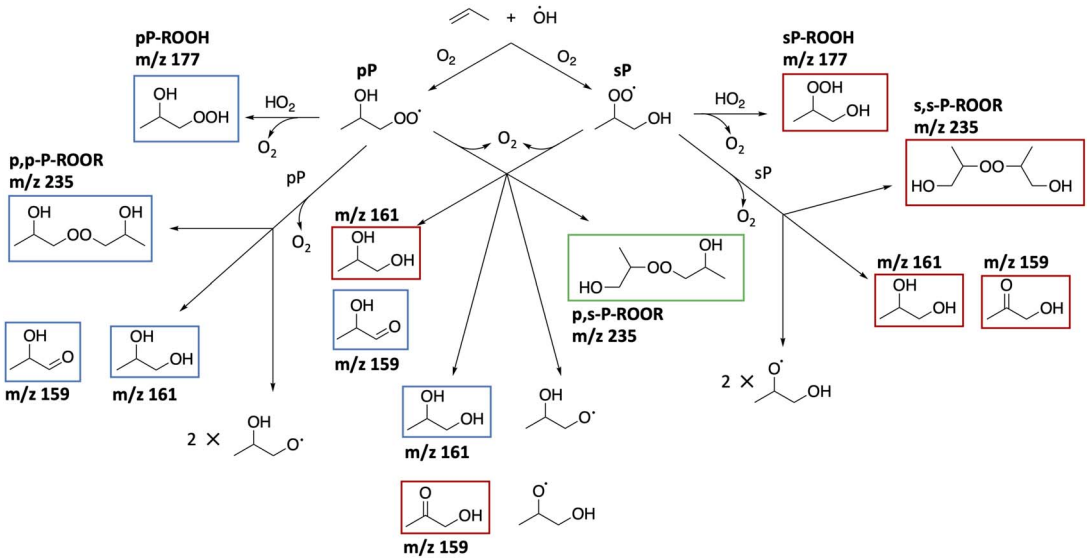


Scheme 3 Reaction scheme for the oxidation of propene by OH in the presence of $O_2$. Stable products that can be observed with the $CF_3O^-$ GC-CIMS are boxed and color-coded such that products that are derived from the primary peroxy radical are in blue, those derived from the secondary peroxy radicals are in red, and products formed from the cross-reactions of the primary and secondary peroxy radicals are in green. Each product is labelled with the *m/z* of that product in our CIMS, which is equal to the molecular weight + 85. In the presence of $O_2$, the alkoxy radicals will form formaldehyde, acetaldehyde, and $HO_2$.

propene-derived hydroxyperoxy radical are generated in the reaction of propene and OH: a primary peroxy radical (pP) *via* the minor addition pathway and a secondary peroxy radical (sP) in the major addition pathway. Similarly to the methylpropene system, at sufficiently high $HO_2/RO_2$ concentrations $\left(\frac{HO_2}{RO_2} > 2\right)$ the distribution of the ROOH isomers (that derived from the primary peroxy radical, pP-ROOH, and that derived from the secondary peroxy radical, sP-ROOH) is expected to match that of the relative formation rates of pP and sP. This is consistent with the measured isomer distribution in the high $HO_2$ experiment, with an observed distribution of 35%/65% for pP-ROOH/sP-ROOH (Fig. 3c), which is within 5% of the distribution measured in Teng *et al.* (40(±3)%/60(±3)% for pP-ROOH/sP-ROOH).[42]

This distribution diverges from the relative production rates of the peroxy radical isomers in experiments with high $RO_2/HO_2$ ratios $\left(\frac{HO_2}{RO_2} < 1\right)$, exhibiting a distribution of 16%/84% for pP-ROOH/sP-ROOH (Fig. 3a). The change in the distribution demonstrates, as expected, that pP undergoes self- and cross-reaction more quickly than sP. However, the perturbation is smaller than that observed for the distribution of pMP-ROOH and tMP-ROOH, suggesting that the difference in self- and cross-reaction rates between the tertiary and primary peroxy radicals is larger than that between the secondary and primary peroxy radicals. This is consistent with previous observations that the reactivity with respect to self- and cross-reaction decreases with increasing peroxy radical substitution.

As in the methylpropene oxidation system, the isomer distribution of the propene-derived accretion products (p,p-P-ROOR, p,s-P-ROOR, and s,s-P-ROOR) is influenced by the competing effects of the peroxy radical distribution and the self- and cross-reaction rate coefficients. However, the differences in these quantities across the peroxy radical isomers are smaller in the propene system than in the 2-methylpropene system. In experiments with high $RO_2/HO_2$ ratios, the accretion product formed in the cross-reaction of the primary and secondary peroxy radicals is most prominent, and is present in an average proportion of 56% (Fig. 3b). On the other hand, the p,p-P-ROOR and s,s-P-ROOR compounds are present in similar proportions, with an average distribution of 26%/18% for p,p-P-ROOR/s,s-P-ROOR.

In the high $HO_2$ system, the proportion of the total ROOR signal that is composed of s,s-P-ROOR decreases to 11(±2)% on average. This is an effect similar to that observed in the high $HO_2$ regime of the 2-methylpropene system, in which the fraction of t,t-MP-ROOR dramatically decreases due to the reaction of tMP with ethene-derived peroxy radicals. This suggests that sP also preferentially reacts with ethene-derived peroxy radicals over reaction with pP or sP, although this difference between reactivity in the cross-reaction *versus* the self-reaction is less pronounced than that observed for the tertiary peroxy radical. Further, two peaks are observed at the mass of an accretion product formed in the cross-reaction of ethene-derived peroxy radicals and propene-derived peroxy radicals (*m/z* 221). These are produced with an average distribution of 63%/37%. We assign the more prominent peak to pP,E-ROOR (the accretion product formed in the self-reaction of pP with ethene-derived peroxy radicals). The production rates of these and other products are quantified and discussed further in the next section. Similarly to the *cis*-2-butene system, we expect ROOR compounds from combinations of propene-derived $RO_2$ to be composed of several stereoisomers, as each contains two chiral

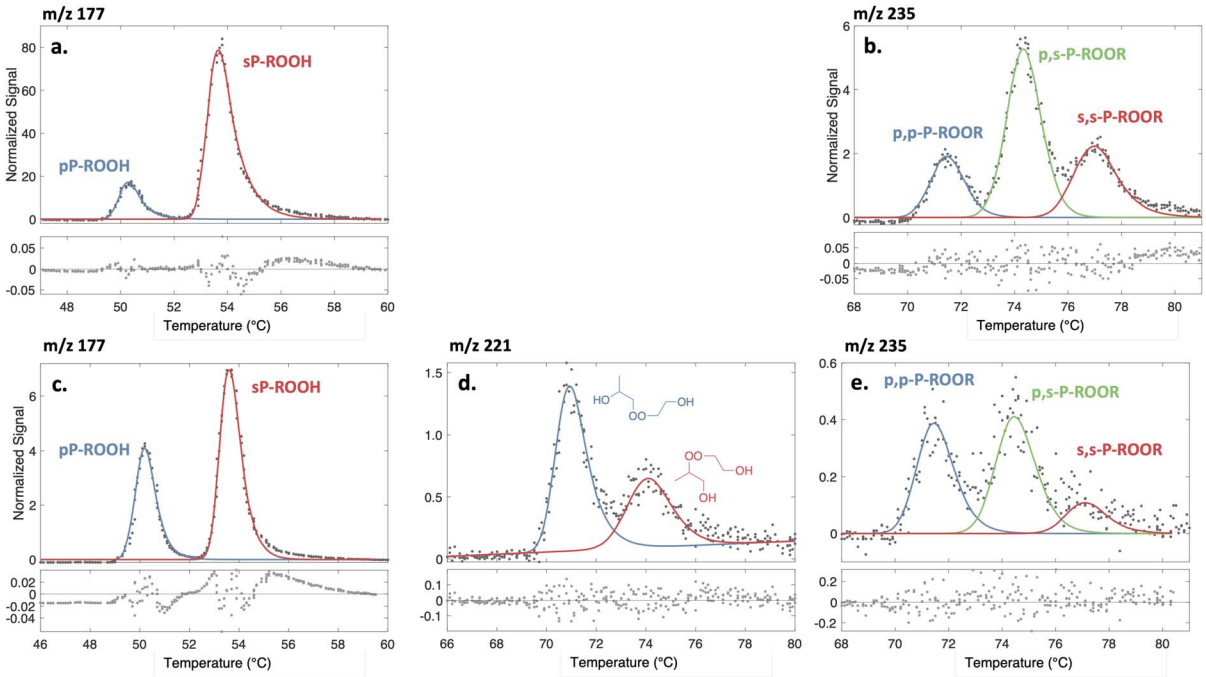


Fig. 3 Gas chromatograms of several important compounds produced in the oxidation of propene by OH in the presence of $O_2$ and ethene, including the ROOH (a and c), the ROOR formed in the self-reaction (b and e), and the ROOR formed in the cross-reaction with ethene (d). Chromatograms in the top row (a and b) are from experiments with high $RO_2/HO_2$ ratios, while those in the bottom row (c, d, and e) are from experiments with high $HO_2/RO_2$ ratios that also included ethene. The bootstrapped best-fits of the relevant peaks are plotted in colored lines on top of the GC traces, and structures are given for the assignments of these peaks. Below each chromatogram the residuals of the best fits are plotted as fractions of the maximum peak signal.

centers. However, we only observe a single peak for each structural isomer, which may indicate our inability to separate these species.

### 3.4 ROOR formation rate coefficients

**3.4.1 Self-reactions.** The formation rate coefficients of the accretion products in these alkene oxidation systems ($k_2\alpha_{2d}$) were measured relative to the formation rate coefficient of the ethene-derived accretion product, as described in the Methods section. The resulting $k_2\alpha_{2d}$ values for the self- and cross-reactions of the peroxy radical isomers formed in the 2-methylpropene, propene, and *cis*-2-butene oxidation systems (and the relevant cross-reactions with ethene-derived peroxy radicals, pE) are given in Table 1.

In Fig. 4, the measured $k_2\alpha_{2d}$ values for each of the self-reactions are plotted in circles as a function of the sum of the total number of heavy atoms in both of the participating peroxy radicals (C + O − 4) and color-coded by peroxy radical substitution. The formation rate coefficient of the accretion product in the self-reaction decreases by approximately one order of magnitude for each additional increase in peroxy radical substitution, with the formation of the ROOR being the fastest for primary peroxy radical self-reactions (on the order of $10^{-13}$ $cm^3$ $molecule^{-1}$ $s^{-1}$) and the slowest for the tertiary peroxy radical self-reaction (on the order of $10^{-15}$ $cm^3$ $molecule^{-1}$ $s^{-1}$). This observation is consistent with the general observation that the overall rate of the self-reaction decreases with increasing peroxy radical substitution[7,11] and suggests that, at least for small alkene-derived hydroxy peroxy radicals, $k_2\alpha_{2d}$ depends primarily on peroxy radical substitution.

Of the systems studied here, the self-reaction rate coefficients for the reactions of the sB,[5] pMP,[6,46] and tMP peroxy radicals[45] have been measured in prior studies. For these systems, we use the $k_2\alpha_{2d}$ measured in this work and the literature value for the rate coefficient ($k_{2,meas}$ in column 4 of Table 1) to estimate $\alpha_{2d}$, the branching fraction to the formation of the accretion product. These values are given in column 6 of Table 1. We can further estimate $\alpha_{2d}$ for the propene-derived peroxy radical isomers using measured rate coefficients for peroxy radicals with similar structures – these estimates are given in Table 1 as well (this is discussed in more detail below). The estimated $\alpha_{2d}$ values for $C_4$ peroxy radical self-reactions, which encompass primary, secondary, and tertiary peroxy radicals, have significantly overlapping uncertainties. However, these values suggest that $\alpha_{2d}$ decreases with increasing radical substitution. This trend is also observed for $C_3$ peroxy radicals, but with only two points this trend is uncertain. Clearly, further studies are needed to explore the relationship between structure and $\alpha_{2d}$. The substitution trend observed here is opposite that reported in a recent study of small alkyl peroxy radicals, which suggests that the branching fraction to accretion product formation increases with increasing alkyl radical substitution.[30] Future work should explore the relationship between peroxy

Table 1 The measured $k_2\alpha_{2d}$ values for each of the systems in this study. Peroxy radicals are colored by subtitution as in Fig. 4

| Reactants | Type[h] | $k_2\alpha_{2d}$ ($\times10^{-13}$) cm$^3$ molec$^{-1}$ s$^{-1}$ | $k_{2,meas}$ ($\times10^{-13}$) cm$^3$ molec$^{-1}$ s$^{-1}$ | $k_{2,ar}$[g] ($\times10^{-13}$) cm$^3$ molec$^{-1}$ s$^{-1}$ | Implied $\alpha_{2d}$ |
|---|---|---|---|---|---|
| **Ethene** | | | | | |
| $HOCH_2CH_2O_2$ + $HOCH_2CH_2O_2$ | p + p | 5.5(±2.6)[a] | 24(±10) | | 0.23(±0.05) |
| **Propene** | | | | | |
| $CH_3CH(OH)CH_2O_2$ + $CH_3CH(OH)CH_2O_2$ | p + p | 4.8 | 24[e] | | 0.20 |
| $CH_3CH(O_2)CH_2OH$ + $CH_3CH(O_2)CH_2OH$ | s + s | 0.35 | 5.0[f] | | 0.07 |
| $CH_3CH(O_2)CH_2OH$ + $CH_3CH(OH)CH_2O_2$ | s + p | 2.6 | | 15 | 0.17 |
| $CH_3CH(OH)CH_2O_2$ + $HOCH_2CH_2O_2$ | p + p | 8.0 | | 24 | 0.33 |
| $CH_3CH(O_2)CH_2OH$ + $HOCH_2CH_2O_2$ | s + p | 2.5 | | 15 | 0.17 |
| ***Cis*-2-butene** | | | | | |
| $CH_3CH(OH)CH(O_2)CH_3$ + $CH_3CH(OH)CH(O_2)CH_3$ | s + s | 0.19 | 5.0(±1.1)[b] | | 0.04(±0.03) |
| $CH_3CH(OH)CH(O_2)CH_3$ + $HOCH_2CH_2O_2$ | s + p | 1.5 | | 15(±8) | 0.10(±0.05) |
| **2-Methylpropene** | | | | | |
| $(CH_3)_2C(OH)CH_2O_2$ + $(CH_3)_2C(OH)CH_2O_2$ | p + p | 3.9 | 51(±34)[c] | | 0.08(±0.06) |
| $(CH_3)_2C(O_2)CH_2OH$ + $(CH_3)_2C(O_2)CH_2OH$ | t + t | 0.0080 | 0.15(±0.05)[d] | | 0.05(±0.03) |
| $(CH_3)_2C(OH)CH_2O_2$ + $(CH_3)_2C(O_2)CH_2OH$ | p + t | 0.79 | | 26(±19.5) | 0.03(±0.02) |
| $(CH_3)_2C(OH)CH_2O_2$ + $HOCH_2CH_2O_2$ | p + p | 12 | | 38(±30) | 0.32(±0.30) |
| $(CH_3)_2C(O_2)CH_2OH$ + $HOCH_2CH_2O_2$ | t + p | 0.54 | | 12(±6.4) | 0.05(±0.04) |

[a] All values in this row are from Murphy *et al.* 2023.[25] [b] Jenkin and Hayman 1995.[5] The value reported in Jenkin and Hayman is given as a range of possible values between $3.9\times10^{-13}$ cm$^3$ molec$^{-1}$ s$^{-1}$ and $6.0\times10^{-13}$ cm$^3$ molec$^{-1}$ s$^{-1}$. A value in the middle of this range is reported here and used to estimate $\alpha$. [c] Boyd *et al.* 1996.[6] [d] Boyd *et al.* 2003.[45] [e] Value estimated using measured self-reaction rate coefficient for ethene-derived hydroxy peroxy radicals. [f] Value estimated using the measured self-reaction rate coefficient for *cis*-2-butene-derived hydroxy peroxy radicals. [g] Cross-reaction rate coefficients calculated using the arithmetic mean of measured or estimated $k_2$ values. [h] Substitution of the participating peroxy radicals, where p = primary, s = secondary, and t = tertiary $RO_2$.

radical functionalization and branching to accretion product formation.

Although $k_2$ for the propene-derived peroxy radicals have not been measured to our knowledge, we estimate values for $k_2$ for the self-reactions of pP and sP using those values measured for other peroxy radical systems with the same substitution. We assign a value of $k_2$ for the self-reaction of pP approximately equal to that found for the ethene-derived peroxy radical self-reaction ($k_2 = 2.4\times10^{-12}$ cm$^3$ molec$^{-1}$ s$^{-1}$). For the self-reaction of sP, we assign a value of $k_2$ equal to that found for the *cis*-2-butene peroxy radical self-reaction ($k_2 = 5.0\times10^{-13}$ cm$^3$ molec$^{-1}$ s$^{-1}$). This yields estimated branching fractions ($\alpha_{2d}$) of 0.20 for the self-reaction of pP and 0.07 for the self-reaction of sP using the $k_2\alpha_{2d}$ values measured here.

**3.4.2 Cross-reactions.** Table 1 also reports the measured $k_2\alpha_{2d}$ values for the cross reactions of the studied peroxy radicals. These values are plotted in Fig. 4 as squares, with each half of the squares colored by the substitution of one of the participating peroxy radicals. It is interesting to note that these values are quite fast for cross-reactions involving ethene-derived peroxy radicals as a co-reactant (Fig. 4). In general, the formation of the accretion product in the cross-reactions of secondary or tertiary peroxy radicals with primary peroxy radicals is faster than the formation of the accretion product in the corresponding self-reactions. The relationship between $k_2\alpha_{2d}$ for the cross-reactions and the corresponding self-reactions is explored in Fig. 5 for the systems studied in this work (blue squares). The same relationship between the self- and cross-reaction rate coefficients is shown for data reported in Jenkin *et al.* (red circles).[11]

Fig. 5 shows that, for both the $k_2\alpha_{2d}$ values measured in this work and the total $k_2$ values given in Jenkin *et al.*, the cross-reaction rate coefficients correlate well with the arithmetic mean of the corresponding self-reaction rate coefficients (eqn (11)):

$$k_{2,R+R',ar} = \frac{k_{2,R} + k_{2,R'}}{2} \quad (11)$$

This suggests that the arithmetic mean of the self-reaction rate coefficients is a reasonable estimate of the cross-reaction rate coefficients. There is a clear outlier in this trend, the cross-reaction of the tert-butylperoxy radical (t-$C_4H_9O_2$) with the methyl peroxy radical ($CH_3O_2$). However, the recommended rate

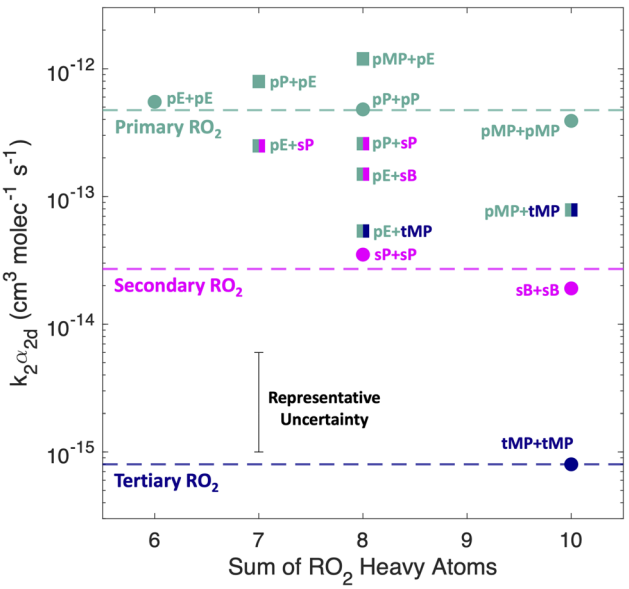


Fig. 4 Measured values of $k_2\alpha_{2d}$ for the self-reactions of the ethene, methylpropene, propene, and *cis*-2-butene-derived peroxy radical systems, plotted as a function of the sum of the number of heavy atoms in the participating peroxy radicals and colored by substitution of the peroxy radical. Dashed lines give the average value of $k_2\alpha_{2d}$ for each of the primary, secondary, and tertiary peroxy radical groups. Squares give $k_2\alpha_{2d}$ values for the cross-reactions measured in this work. All points are labeled with the participating peroxy radicals.

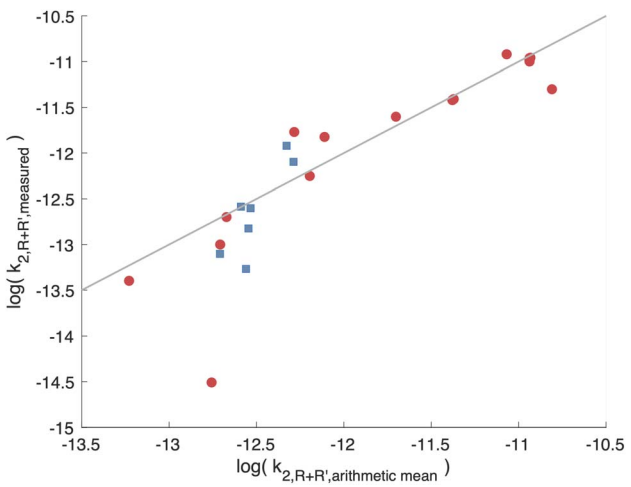


Fig. 5 The relationship between the cross-reaction rate coefficients and the arithmetic mean of the self-reaction rate coefficients ($k_2$) for the peroxy radical systems given in Jenkin *et al.* 2019 (red circles), and the same relationship between $k_2\alpha_{2d}$ values for the cross- and self-reactions examined in this study (blue squares). The solid gray line denotes the 1 : 1 line.

coefficient for this reaction is fairly uncertain ($\Delta \log k = 0.6$), with only two reported measurements.[31,47,48]

Using the arithmetic mean of the measured/estimated rate coefficients for the self-reactions ($k_{2,ar}$ in column 5 of Table 1), we also estimate $\alpha_{2d}$ for each of the cross reactions, and these estimated values are shown in Table 1. Similarly to the $k_2\alpha_{2d}$ values, these values tend to lie in between the $\alpha_{2d}$ values of the corresponding self-reactions, with the notable exception of the self-reaction of pP with *E*, which has a significant implied $\alpha_{2d}$ of 0.33.

# 4 Conclusion

The formation rate coefficient of the accretion product depends largely on the substitution of the peroxy radical and decreases by an order of magnitude with increasing substitution. The branching fraction to the formation of the accretion product ranges between 0.03 and 0.33, and decreases with increasing radical substitution for $RO_2$ of the same carbon number. Further, the formation of the accretion product in the cross-reaction systems yielded formation rate coefficients that are well-described by the arithmetic mean of the corresponding self-reactions. These relationships should be studied further and utilized in the estimation of peroxy radical rate coefficients in models of atmospheric chemical mechanisms.

# Conflicts of interest

There are no conflicts to declare.

# Data availability

Data for this article, including raw time series data and instrument parameters for each experiment, are available at CaltechData at **https://doi.org/10.22002/77v95-gpt71**.

Supplementary information: experimental and instrumental conditions, experimental results, sensitivities, and additional comments regarding procedures and conclusions presented in the main body. See DOI: **https://doi.org/10.1039/d5ea00106d**.

# Acknowledgements

This material is based upon work supported by the U. S. National Science Foundation under Grant No. CHE-1905340 and Grant No. CHE-2305204. This work was also supported by Villum Fonden (VIL50443).

# References

1 R. Atkinson, *J. Phys. Chem. Ref. Data*, 1997, **26**, 215–290.
2 P. D. Lightfoot, R. A. Cox, J. N. Crowley, M. Destriau, G. D. Hayman, M. E. Jenkin, G. K. Moortgat and F. Zabel, *Atmos. Environ. Gen. Top*, 1992, **26**, 1805–1961.
3 M. E. Jenkin and K. C. Clemitshaw, *Atmos. Environ.*, 2000, **34**, 2499–2527.
4 G. S. Tyndall, R. A. Cox, C. Granier, R. Lesclaux, G. K. Moortgat, M. J. Pilling, A. R. Ravishankara and T. J. Wallington, *J. Geophys. Res. Atmos.*, 2001, **106**, 12157–12182.
5 M. E. Jenkin and G. D. Hayman, *J. Chem. Soc., Faraday Trans.*, 1995, **91**, 1911–1922.
6 A. A. Boyd, R. Lesclaux, M. E. Jenkin and T. J. Wallington, *J. Phys. Chem.*, 1996, **100**, 6594–6603.

7 J. J. Orlando and G. S. Tyndall, *Chem. Soc. Rev.*, 2012, **41**, 6294–6317.
8 J. H. Seinfeld and S. N. Pandis, *Atmospheric Chemistry and Physics : from Air Pollution to Climate Change*, Wiley, Hoboken, New Jersey, 2016.
9 A. E. Perring, S. E. Pusede and R. C. Cohen, *Chem. Rev.*, 2013, **113**, 5848–5870.
10 J. D. Crounse, L. B. Nielsen, S. Jørgensen, H. G. Kjaergaard and P. O. Wennberg, *J. Phys. Chem. Lett.*, 2013, **4**, 3513–3520.
11 M. E. Jenkin, R. Valorso, B. Aumont and A. R. Rickard, *Atmos. Chem. Phys.*, 2019, **19**, 7691–7717.
12 O. US EPA, National Air Quality: Status and Trends of Key Air Pollutants, 2014, **https://www.epa.gov/air-trends**.
13 S. L. Winkler, J. E. Anderson, L. Garza, W. C. Ruona, R. Vogt and T. J. Wallington, *npj Clim. Atmos. Sci.*, 2018, **1**, 1–5.
14 P. O. Wennberg, K. H. Bates, J. D. Crounse, L. G. Dodson, R. C. McVay, L. A. Mertens, T. B. Nguyen, E. Praske, R. H. Schwantes, M. D. Smarte, J. M. St Clair, A. P. Teng, X. Zhang and J. H. Seinfeld, *Chem. Rev.*, 2018, **118**, 3337–3390.
15 A. C. Ziola and P. J. Ziemann, *J. Phys. Chem.*, 2025, **129**, 1688–1703.
16 R. Lee, G. Gryn'ova, K. U. Ingold and M. L. Coote, *Phys. Chem. Chem. Phys.*, 2016, **18**, 23673–23679.
17 R. R. Valiev, G. Hasan, V.-T. Salo, J. Kubečka and T. Kurten, *J. Phys. Chem.*, 2019, **123**, 6596–6604.
18 C. M. Kenseth, Y. Huang, R. Zhao, N. F. Dalleska, J. C. Hethcox, B. M. Stoltz and J. H. Seinfeld, *Proceedings of the National Academy of Sciences*, 2018, 115, 8301–8306.
19 O. Peräkylä, T. Berndt, L. Franzon, G. Hasan, M. Meder, R. R. Valiev, C. D. Daub, J. G. Varelas, F. M. Geiger, R. J. Thomson, M. Rissanen, T. Kurtén and M. Ehn, *J. Am. Chem. Soc.*, 2023, **145**, 7780–7790.
20 T. Berndt, B. Mentler, W. Scholz, L. Fischer, H. Herrmann, M. Kulmala and A. Hansel, *Environ. Sci. Technol.*, 2018, **52**, 11069–11077.
21 U. Molteni, M. Simon, M. Heinritzi, C. R. Hoyle, A.-K. Bernhammer, F. Bianchi, M. Breitenlechner, S. Brilke, A. Dias, J. Duplissy, C. Frege, H. Gordon, C. Heyn, T. Jokinen, A. Kürten, K. Lehtipalo, V. Makhmutov, T. Petäjä, S. M. Pieber, A. P. Praplan, S. Schobesberger, G. Steiner, Y. Stozhkov, A. Tomé, J. Tröstl, A. C. Wagner, R. Wagner, C. Williamson, C. Yan, U. Baltensperger, J. Curtius, N. M. Donahue, A. Hansel, J. Kirkby, M. Kulmala, D. R. Worsnop and J. Dommen, *ACS Earth Space Chem.*, 2019, **3**, 873–883.
22 A. J. Kwan, A. W. H. Chan, N. L. Ng, H. G. Kjaergaard, J. H. Seinfeld and P. O. Wennberg, *Atmos. Chem. Phys.*, 2012, **12**, 7499–7515.
23 T. Berndt, S. Richters, R. Kaethner, J. Voigtländer, F. Stratmann, M. Sipilä, M. Kulmala and H. Herrmann, *J. Phys. Chem.*, 2015, **119**, 10336–10348.
24 B. H. Lee, F. D. Lopez-Hilfiker, E. L. D'Ambro, P. Zhou, M. Boy, T. Petäjä, L. Hao, A. Virtanen and J. A. Thornton, *Atmos. Chem. Phys.*, 2018, **18**, 11547–11562.
25 S. E. Murphy, J. D. Crounse, K. H. Møller, S. P. Rezgui, N. J. Hafeman, J. Park, H. G. Kjaergaard, B. M. Stoltz and P. O. Wennberg, *Environ. Sci.: Atmos.*, 2023, **3**, 882–893.
26 H. Yue, C. Zhang, X. Lin, Z. Wen, W. Zhang, S. Mostafa, P.-L. Luo, Z. Zhang, P. Hemberger, C. Fittschen and X. Tang, *Int. J. Mol. Sci.*, 2023, **24**, 3731.
27 L. Liu, C. Zhang, Y. Xia, W. Zhang, Z. Wang and X. Tang, *Chemosphere*, 2024, **363**, 142846.
28 A. C. Noell, L. S. Alconcel, D. J. Robichaud, M. Okumura and S. P. Sander, Near-Infrared Kinetic Spectroscopy of the $HO_2$ and $C_2H_5O_2$ Self-Reactions and Cross Reactions, *J. Phys. Chem. A*, 2010, **114**(26), 6983–6995.
29 M. Shamas, M. Assali, C. Zhang, X. Tang, W. Zhang, L. Pillier, C. Schoemaecker and C. Fittschen, Rate Constant and Branching Ratio for the Reactions of the Ethyl Peroxy Radical with Itself and with the Ethoxy Radical, *ACS Earth Space Chem.*, 2022, **6**(1), 181–188.
30 B. Nozière, *Chem. Sci.*, 2025, **16**, 16590–16596.
31 R. Atkinson, D. L. Baulch, R. A. Cox, J. N. Crowley, R. F. Hampson, R. G. Hynes, M. E. Jenkin, M. J. Rossi, J. Troe and I. Subcommittee, *Atmos. Chem. Phys.*, 2006, **6**, 3625–4055.
32 K. T. Vasquez, H. M. Allen, J. D. Crounse, E. Praske, L. Xu, A. C. Noelscher and P. O. Wennberg, *Atmos. Meas. Tech.*, 2018, **11**, 6815–6832.
33 F. Paulot, J. D. Crounse, H. G. Kjaergaard, J. H. Kroll, J. H. Seinfeld and P. O. Wennberg, *Atmos. Chem. Phys.*, 2009, **9**, 1479–1501.
34 J. M. St. Clair, K. M. Spencer, M. R. Beaver, J. D. Crounse, F. Paulot and P. O. Wennberg, *Atmos. Chem. Phys.*, 2014, **14**, 4251–4262.
35 J. D. Crounse, F. Paulot, H. G. Kjaergaard and P. O. Wennberg, *Phys. Chem. Chem. Phys.*, 2011, **13**, 13607–13613.
36 N. Hyttinen, R. V. Otkjær, S. Iyer, H. G. Kjaergaard, M. P. Rissanen, P. O. Wennberg and T. Kurtén, *J. Phys. Chem.*, 2018, **122**, 269–279.
37 J. D. Crounse, K. A. McKinney, A. J. Kwan and P. O. Wennberg, *Anal. Chem.*, 2006, **78**, 6726–6732.
38 T. Su and W. J. Chesnavich, *J. Chem. Phys.*, 1982, **76**, 5183–5185.
39 A. L. Garden, F. Paulot, J. D. Crounse, I. J. Maxwell-Cameron, P. O. Wennberg and H. G. Kjaergaard, *Chem. Phys. Lett.*, 2009, **474**, 45–50.
40 T. O'Haver, Interactive Peak Fitter, 2017, **https://terpconnect.umd.edu/toh/spectrum/InteractivePeakFitter.htm**.
41 S. W. Sharpe, R. L. Sams and T. J. Johnson, *Proceedings of the 31st Applied Image Pattern Recognition Workshop on from Color to Hyperspectral: Advancements in Spectral Imagery Exploitation*, USA, 2002, pp. 45–48.
42 A. P. Teng, J. D. Crounse, L. Lee, J. M. St. Clair, R. C. Cohen and P. O. Wennberg, *Atmos. Chem. Phys.*, 2015, **15**, 4297–4316.
43 L. Xu, K. H. Møller, J. D. Crounse, R. V. Otkjær, H. G. Kjaergaard and P. O. Wennberg, *J. Phys. Chem.*, 2019, **123**, 1661–1674.

44 G. Hasan, V.-T. Salo, R. R. Valiev, J. Kubečka and T. Kurtén, *J. Phys. Chem.*, 2020, **124**, 8305–8320.
45 A. A. Boyd, E. Villenave and R. Lesclaux, *Atmos. Environ.*, 2003, **37**, 2751–2760.
46 A. Chakir, J. P. Ganne, E. Roth, J. Brion and D. Daumont, *Phys. Chem. Chem. Phys.*, 2004, **6**, 3389–3395.
47 D. Parkes, *15th International Symposium on Combustion*, The Combustion Institute, Pittsburgh, 1975, p. 795.
48 D. A. Osborne and D. J. Waddington, *J. Chem. Soc., Perkin Trans. 2*, 1984, 1861–1867.